Ab Initio Studies of ClO_x Reactions. 3. Kinetics and Mechanism for the OH + OClO Reaction

Zhen-Feng Xu, Rongshun Zhu, and M. C. Lin*

Department of Chemistry, Emory University, Atlanta, Georgia 30322

Received: May 9, 2002; In Final Form: November 11, 2002

The mechanism for the OH + OClO reaction on the singlet and triplet surfaces and its rate constants for formation of various products have been investigated by means of ab initio molecular orbital theory and variational RRKM theory calculations. The geometric parameters of stationary points were optimized at the B3LYP level of theory with the 6-311G(d,p) and 6-311+G(3df,2p) basis sets, and the potential energy surfaces were evaluated at the G2M(CC2)//B3LYP/6-311+G(3df,2p) level of theory. Three main product channels, all located on the singlet PES, have been identified: (1) HOO + ClO, (2) HOCl + $^1O_2$, and (3) $HOClO_2$, the association product. The predicted results show that the rate constants for channels 1 and 2 are pressure-independent up to 1000 atm and that for channel 3 is strongly pressure dependent. Below 1000 K, all rate constants were found to vary negatively with temperature. The individual and total rate constants in the temperature range from 200 to 1000 K at 1 Torr He pressure can be represented by $k_1(T) = 1.22 \times 10^{-22}T^{2.75}$ exp(1682/*T*), $k_2(T) = 5.47 \times 10^{-20}T^{2.07}$ exp(2064/*T*), $k_3(T) = 1.37 \times 10^{4}T^{-6.61}$ exp(−536/*T*) (200−500 K) and $4.99 \times 10^{54}T^{-22.36}$ exp(−9807/*T*) (500−1000 K), and $k_{tot}(T) = 1.78 \times 10^{-20}T^{2.25}$ exp(2100/*T*) in units of cm^3 $molecule^{-1}$ s^{-1}. The predicted rate constant, with the HOCl + $^1O_2$ as the major products in the 300−500 K range, agrees well with available experimental data obtained at 1 Torr He pressure. The high- and low-pressure limits of k_3 can be effectively given by $k_3^{\infty}(T) = 3.24 \times 10^{-11}T^{0.28}$ exp(−18/*T*) cm^3 $molecule^{-1}$ s^{-1} in 200−2500 K and $k_3°(T) = 1.28 \times 10^{-13}T^{-6.36}$ exp(−635/*T*) for 200−800 K, $7.37 \times 10^{84}T^{-36.02}$ exp(−22134/*T*) for 800−1000 K, and $2.91 \times 10^{-13}T^{-8.42}$ exp(11500/*T*) for 1000−2500 K in units of cm^6 $molecule^{-2}$ s^{-1} with N_2 as the third body.

1. Introduction

Chlorine dioxide, OClO, is a key reactive intermediate in the combustion of ammonium perchlorate (AP); it may be formed by the decomposition of ClO_3[1] and by the reaction of OH with ClO_3, which has been predicted to yield HO_2 + OClO very effectively.[2] In the stratosphere, OClO may be formed by the reaction of ClO with XO (where X = Br, Cl, or O_2).[3,4] In both media, OH radicals are known to be present and play a key role in the global kinetics. Poulet, Zagogianni, and Le Bras[5] investigated experimentally the kinetics of reaction of OH with OClO by electron paramagnetic resonance and laser-induced fluorescence in 1986. They obtained total rate constants at pressures 0.5−1.4 Torr and over the temperature range from 293 to 473 K and suggested the following reaction mechanism:

$$OH + OClO \rightarrow HOO + ClO$$

$$OH + OClO \rightarrow HOCl + O_2$$

$$HOO + ClO \rightarrow HOCl + O_2$$

to explain an unusually high HOCl + O_2 product yield with its branching ratio approaching unity, according to the result of their kinetic modeling.[5] In addition to the above processes, the association reaction,

$$OH + OClO \rightarrow HOClO_2$$

which has not been considered under the low-pressure conditions employed,[5] may become competitive under the stratospheric condition.

In the present work, we investigate the kinetics and mechanism of the title reaction by high-level molecular orbital and statistical theory calculations using a similar approach as we have recently employed in our studies of analogous systems, OH + ClO,[6] O + OClO,[7] OH + ClO_3,[2] and ClO + ClO.[8] The results from our latest study of this series, OH + OClO, is presented herein.

2. Computational Methods

The geometric parameters of the reactants, products, intermediates, and transition states on the potential energy surfaces of the OH + OClO system at singlet and triplet electronic states were optimized at the B3LYP level of theory[9,10] (i.e., Becke's three-parameter nonlocal exchange functional with the nonlocal correlation functional of Lee, Yang, and Parr) with the standard Gaussian basis sets 6-311G(d,p) and 6-311+G(3df,2p). All the stationary points have been identified for local minima and transition states by vibrational analysis. Intrinsic reaction coordinate analyses[11] have been performed to confirm the connection between transition states and designated reactants, products, or intermediates. The higher level single-point energy calculations of the stationary points were performed by the G2M(CC2) method[12] based on the optimized geometries at the B3LYP/6-311+G(3df,2p) level. The G2M method calculates the base energy at the PMP4/6-311G(d,p) level of theory and improves it with the expanded basis set and coupled cluster

* Corresponding author. E-mail: chemmcl@emory.edu. National Science Council Distinguished Visiting Professor at the National Chiaotung University, Hsinchu, Taiwan.

10.1021/jp021183+ CCC: $25.00
Published on Web 01/25/2003

TABLE 1: Optimized Geometric Parameters of the Reactants and Products (Bond Lengths in Ångstroms and Angles in Degrees)

species		B3LYP/ 6-311G(d,p)	B3LYP/ 6-311+G(3df,2p)	expt
OH ($^2\Pi$)	R_{OH}	0.975	0.974	0.971[a]
OClO ($^2B_1$)	R_{OCl}	1.546	1.479	1.471[a]
	θ_{OClO}	118.1	117.3	117.6
HOO ($^2A''$)	R_{HO}	0.976	0.975	0.971[b]
	R_{OO}	1.328	1.324	1.331
	θ_{HOO}	105.5	105.5	104.3
ClO ($^2\Pi$)	R_{ClO}	1.626	1.576	1.570[a]
HOCl ($^1A'$)	R_{HO}	0.968	0.966	0.964[c]
	R_{OCl}	1.738	1.700	1.689
	θ_{HOCl}	102.1	103.7	103.0
$^1O_2$ ($^1\Delta_g$)	R_{OO}	1.207	1.203	1.216[d]
$^3O_2$ ($^3\Sigma_g^-$)	R_{OO}	1.206	1.203	1.208

[a] Reference 17. [b] Reference 18. [c] Reference 19. [d] Reference 20.

TABLE 2: Moments of Inertia and Vibrational Frequencies of the Reactants and Products Predicted at B3LYP/6-311+G(3df,2p)

species	I_a, I_b, I_c (au)	frequencies (cm^{-1})
OH ($^2\Pi$)	3.2, 3.2	3722 (3735)[a]
OClO ($^2B_1$)	35.3, 182.4, 217.7	451, 966, 1117 (447, 945, 1110)[b]
ClO ($^2\Pi$)	97.3, 97.3	861 (853)[a]
HOCl ($^1A'$)	2.9, 120.3, 123.2	739, 1262, 3786 (725, 1267, 3794)[c]
HOO ($^2A''$)	2.9, 53.2, 56.1	1172, 1443, 3612 (1098, 1392, 3436)[d]
$^1O_2$ ($^1\Delta_g$)	41.3, 41.3	1634 (1509)[b]
$^3O_2$ ($^3\Sigma_g^-$)	41.3, 41.3	1645 (1580)[b]

[a] Reference 20. [b] Reference 17. [c] Reference 21. [d] Reference 22.

corrections as well as a "higher level correction". All electronic structure calculations were performed with the GAUSSIAN 98 program.[13]

The rate constant for the association reaction producing $HOClO_2$ was calculated by the VARIFLEX program[14] based on the microcanonical Rice−Ramsperger−Kassel−Marcus (RRKM) theory.[15] The component rates were evaluated at the E/J-resolved level and the pressure dependence was treated by the one-dimensional master equation calculations using the Boltzmann probability of the complex for the J-distribution. For the barrierless transition state process, the Morse functional

$$V(R) = D_e\{1 - \exp[-\beta(R - R_e)]\}^2$$

was used to represent the minimum potential energy path for the association reaction. Here, D_e is the bonding energy excluding zero-point vibrational energy for an association reaction, R is the reaction coordinate (i.e., the distance between the two bonding atoms), and R_e is the equilibrium value of R at the stable intermediate structure.

For the coupling of different accessible reaction paths, we have employed the ChemRate program of NIST[16] to evaluate product branching ratios under different T, P conditions. The predicted rate constants and product branching ratios will be compared with experimental values.[5]

3. Results and Discussion

A. Potential Energy Surfaces and Reaction Mechanism. The geometries of the intermediates optimized at the B3LYP/6-311G(d,p) and B3LYP/6-311+G(3df,2p) level are shown in Figure 1 whereas those of the transition states optimized at the same levels are displayed in Figure 2. The singlet and triplet potential energy diagrams obtained at the G2M level are presented in Figure 3a,b. Tables 1 and 2 display the calculated geometry parameters and frequencies, comparing with available experimental values for the reactants and products. The total and relative energies of the singlet and triplet species involved in the reaction are compiled in Table 3, and the vibrational frequencies and moments of inertia are summarized in Table 4 for the intermediates and transition states. Table 5 compares the experimental and calculated heats of formation for some known species.

By inspection of Table 1, one can see that the structural parameters of the all species obtained at the B3LYP/6-311+G(3df,2p) level are in better agreement with experimental values than those at the B3LYP/6-311G(d,p) level. The largest errors in bond length and angle are 0.075 Å and 1.2° at the B3LYP/6-311G(d,p) level, and 0.011 Å and 1.2° at the B3LYP/6-311+G(3df,2p) level. For the predicted frequencies listed in Table 2, the largest deviation from experimental values is 8%. The intermediates and transition states on the singlet and triplet paths will be discussed in the following sections.

(a) Singlet reaction channels. (i) ^{1}HOOClO-1 and ^{1}HOOClO-2 (Two Isomers of Peroxychlorous Acid) and $^1HOClO_2$ (Chloric Acid). It is readily seen that the interaction between the O atom of OH and the O or Cl atom of OClO directly forms different intermediates, HOOClO and $HOClO_2$. HOOClO has both isomers as shown in Figure 1. Checking the structure parameters of ^{1}HOOClO-1 and ^{1}HOOClO-2 we find that the Cl2−O3 bond lengths (see Figure 1) for both intermediates are sensitive to the size of the basis set. At the B3LYP/6-311+G(3df,2p) level, this bond in ^{1}HOOClO-1 and ^{1}HOOClO-2 decreases by 0.171 and 0.521 Å, respectively, comparing with those obtained at the B3LYP/6-311G(d,p) level; meanwhile, the dihedral angles O4O3Cl2O1 and H5O4O3Cl2 in ^{1}HOOClO-1 increase by about 5° when the basis set increases from 6-311G(d,p) to 6-311+G(3df,2p). In ^{1}HOOClO-2, however, the dihedral angle changes are more significant, they increase by 70.5° and 11.3° from the 6-311G(d,p) to the 6-311+G(3df,2p) for the O4O3Cl2O1 and H5O4O3Cl2 dihedral angles, respectively. The absolute values of the Cl2−O3 bond and the O4O3Cl2O1 and H5O4O3Cl2 dihedral angles in ^{1}HOOClO-1 obtained at the B3LYP/6-311+G(3df,2p) level, 1.750 Å, 80.4°, and 93.1°, respectively, are close to those of 1.758 Å, 78.2°, and 93.8° obtained at the MP2/6-311G(2df,2p) level by Francisco and Sander.[24]

For the $HOClO_2$ intermediate, with the basis set size increasing, significant structural changes also occur in the bond lengths and dihedral angles. The O1−Cl2, O3−Cl2, and Cl2−O4 bonds decrease by 0.034, 0.047, and 0.051 Å, respectively; whereas the dihedral O1Cl2O4H5 increases from −59.9° to +21.7° and the dihedral O3Cl2O4H5 increases from 59.4° to 140.7°, when the basis set increases from 6-311G(d,p) to 6-311+G(3df,2p). Similar trends were found in the structures obtained from the MP2/6-31G(d) to MP2/6-311G(2df,2p) levels by Francisco and Sander.[24]

^{1}HOOClO-1, ^{1}HOOClO-2, and $^1HOClO_2$ lie below the reactants by −12.1, −13.9, and −32.6 kcal/mol, respectively, at the G2M//B3LYP/6-311+G(3df,2p) level. Among these, chloric acid is the most stable one, which is also consistent with the results obtained by Francisco and Sander.[24] Because the structures optimized using larger basis sets are more reliable, in the following text, the cited geometric parameters are those obtained at the B3LYP/6-311+G(3df,2p) level and the G2M energies on the basis of the structures at this level.

(ii) Isomerization among ^{1}HOOClO-1, ^{1}HOOClO-2, and $^1HOClO_2$. The transition states (TS1 and TS2) and energy diagram for isomerization of ^{1}HOOClO-1 to ^{1}HOOClO-2 and $^1HOClO_2$, are shown in Figures 2 and 3a, respectively. For the

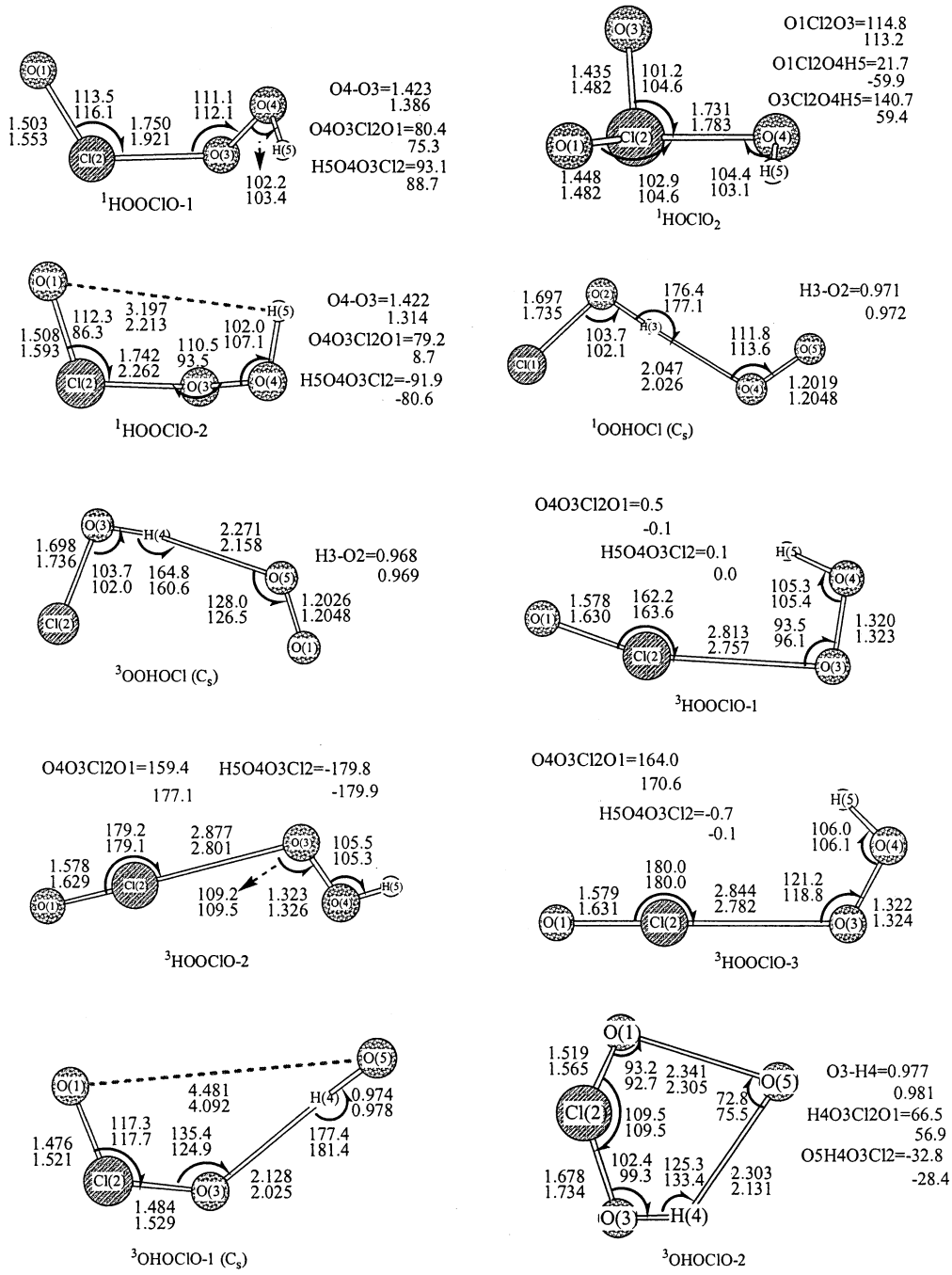

Figure 1. Optimized geometries of the intermediates (lengths in ångstroms and angles in degrees). The top numbers were optimized at the B3LYP/6-311+G(3df,2p) level; the bottom numbers were optimized at the B3LYP/6-311G(d,p) level.

isomerization between ^{1}HOOClO-1 and ^{1}HOOClO-2, it occurs mainly through the rotation of the OH group along the O3−O4 bond. One can see from Figure 2 that there is only minor variation in the bond lengths and bond angles from ^{1}HOOClO-1 via TS1 to ^{1}HOOClO-2; however, the dihedral angles H5O4O3Cl2 in these three species are +93.1°, −1.0°, and −91.9°, respectively, with significantly larger changes as expected. The isomerization barrier for this process is 5.1 kcal/mol. For the isomerization from ^{1}HOOClO-1 to ^{1}HOClO$_2$, the corresponding transition state TS2, has a three-center configuration. Inspecting the structures of ^{1}HOOClO-1 and TS2, we see that the forming Cl2−O4 bond length in TS2 is 0.305 Å shorter than that in ^{1}HOOClO-1 and the breaking O3−O4 bond in TS2 lengthens by 0.656 Å, comparing with those in ^{1}HOOClO-1; meanwhile, the O4O3Cl2 bond angle bends from 111.1° in ^{1}HOOClO-1 to 83.1° in TS1. Because of the larger configuration changes during the isomerization process, TS2 has a higher barrier, which lies above the reactants by 3.8 kcal/mol at the G2M level.

(iii) HOO + ClO Formation. The fragmentation of the Cl2−O3 bond in ^{1}HOOClO-1 via TS3 results in the formation of HOO + ClO. In TS3, the breaking Cl−O bond increases 0.175 Å whereas the forming O−O bond decreases 0.053 Å, comparing with those in ^{1}HOOClO-1. TS3 lies above the intermediate, ^{1}HOOClO-1, and the products HOO + ClO by 9.4 and 3.6 kcal/mol, respectively (see Figure 3a). This dissociation mechanism is different from that of HOOCl → HOO + Cl, which is a barrierless process and is the dominant channel in the HO + ClO reaction.[6]

(iv) HOCl + ^{1}O$_2$ Formation. There are two reaction channels producing HOCl and ^{1}O$_2$, as shown in Figure 3a. In the first channel, the configuration of ^{1}HOOClO-2 rotates, accompanied

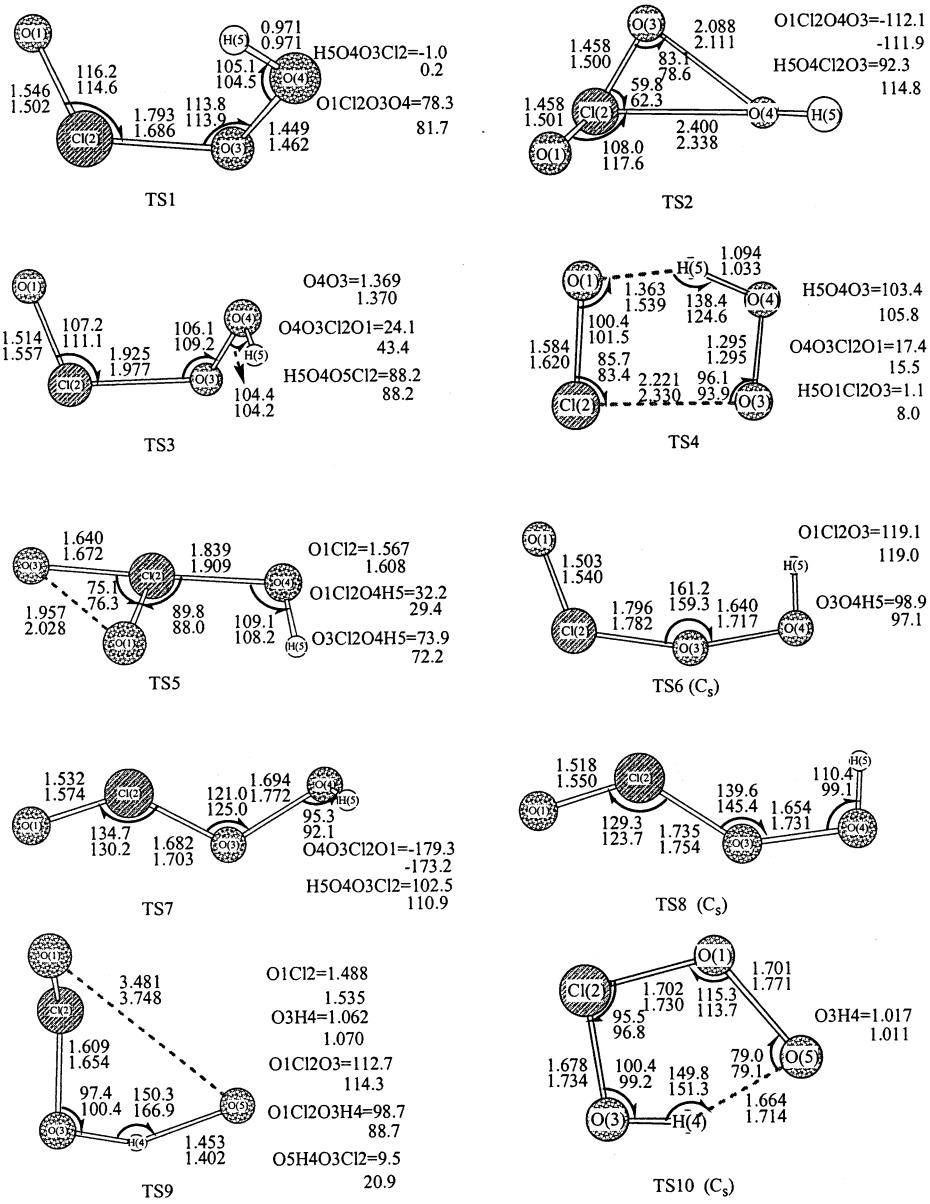

Figure 2. Optimized geometries of the transition states (lengths in ångstroms and angles in degrees). The top numbers were optimized at the B3LYP/6-311+G(3df,2p) level; the bottom numbers were optimized at the B3LYP/6-311G(d,p) level.

by H atom migration to O1 to form the molecular complex ^{1}OOHOCl via a twisted five-membered ring transition state TS4, followed by the decomposition of the complex into HOCl and $^1O_2$ through a barrierless process. The imaginary frequency of TS4 is 789 cm^{-1}, and its vector points to ^{1}OOHOCl positively and to ^{1}HOOClO-2 negatively. At the G2M level, the forward and reverse potential barriers of this reaction channel are 5.7 and 21.0 kcal/mol, respectively. Apparently, it is quite favorable to the forward reaction. ^{1}OOHOCl is a hydrogen-bonded complex formed by the association of HOCl with $^1O_2$; it lies only 2.2 kcal/mol below HOCl and $^1O_2$. For the second channel, the two terminal O atoms of $HOClO_2$ form O_2 and eliminate via TS5. This process involves the breaking of two Cl−O bonds and the formation of one O−O bond. Expectably, this reaction path has large forward and reverse potential barriers, 67.8 and 62.2 kcal/mol, respectively. Apparently, this channel is kinetically unimportant and will have no contribution to the formation of HOCl + $^1O_2$.

(b) Triplet Reaction Channels. (i) HOO + ClO Formation. Three channels were found to form HOO + ClO over the triplet electronic state potential surface. TS6, TS7, and TS8 correspond to one of the O atoms in OClO being abstracted by OH through cis,cis, trans,trans, and trans,cis structures (see Figure 2) to form loose complexes, ^{3}HOOClO-1, ^{3}HOOClO-3, and ^{3}HOOClO-2, respectively. The potential barriers of TS6, TS7, and TS8 at the G2M level are 41.0, 33.0, and 34.4 kcal/mol, as shown in Figure 3b. Similarly, high barriers on the triplet potential energy surface were also found in the HO + ClO[6] and ClO + ClO[8] reactions. For the HO + ClO → ^{3}HOOCl and ClO + ClO → ^{3}ClOOCl reactions; however, their barriers are comparatively lower, at 17.2[6] and 28.0 kcal/mol,[8] respectively. These phenomena may be attributed to the interaction between the two parallel spin electrons on the two radicals, the repulsive interaction results in the energy interval of frontier molecular orbitals being quite large.

(ii) HOCl + $^3O_2$ Formation. The formation of HOCl and $^3O_2$ involves three loose complexes and two tight transition states. This process can be expressed as HO + OClO → ^{3}OHOClO-1 → TS9 → ^{3}OHOClO-2 → TS10 → ^{3}OOHOCl → HOCl + $^3O_2$, as shown in Figure 3b. For TS9, it mainly undergoes the transfer of the H atom in the HO group to one of the terminal O in OClO (see Figure 2) to form complex ^{3}OHOClO-2. In TS10,

TABLE 3: Total and Relative Energies of the Reactants, Intermediates, Transition States, and Products for the OClO + OH Reaction with ZPE Correction

species	energies (kcal/mol) B3LYP/6-311G(d,p)	B3LYP/6-311+G(3df,2p)	G2M//B3LYP/6-311+G(3df,2p)	$\Delta_r H°$(0K) expt[b] (kcal/mol)
OH ($^2\Pi$) + OClO($^2B_1$)	−686.22180[a]	−686.30066[a]	−685.48534[a]	
HOO($^2A''$) + ClO($^2\Pi$)	−32.7	−10.1	−6.3	−7.3
HOCl($^1A'$) + $^1O_2$($^1\Delta_g$)	−39.9	−13.8	−27.0	−27.3
HOCl($^1A'$) + $^3O_2$($^3\Sigma_g^-$)	−78.9	−52.3	−53.4	−49.8
^{1}HOOClO-1	−18.6	−6.2	−12.1	
^{1}HOOClO-2	−23.2	−7.8	−13.9	
^{3}HOOClO-1	−35.3	−11.4	−8.4	
^{3}HOOClO-2	−35.1	−11.4	−7.9	
^{3}HOOClO-3	−34.6	−10.9	−8.3	
^{1}HOClO$_2$	−17.4	−25.3	−32.6	
^{3}OOHOCl($^3A''$)	−79.7	−52.4	−54.6	
^{1}OOHOCl($^1A'$)	−42.5	−15.3	−29.2	
^{3}OHOClO-1($^3A''$)	−3.1	−1.3	−0.5	
^{3}OHOClO-2	31.2	30.8	27.2	
TS1	−14.1	−3.7	−7.0	
TS2	18.8	18.1	3.8	
TS3	−18.3	−3.5	−2.7	
TS4	−23.3	−0.1	−8.2	
TS5	53.3	59.5	35.1	
TS6 ($^3A''$)	15.0	28.7	41.0	
TS7	14.0	26.4	33.6	
TS8 ($^3A''$)	15.1	27.5	34.4	
TS9	18.8	28.4	36.9	
TS10 ($^3A''$)	24.2	43.4	46.7	

[a] Unit in au. [b] References 17, 20, and 23.

TABLE 4: Moments of Inertia and Vibrational Frequencies of the Intermediates and Transition States at the B3LYP/6-311+G(3df,2p) Level

species	I_a, I_b, I_c (au)	frequencies (cm^{-1})
^{1}HOOClO-1	103, 466, 515	137, 255, 356, 432, 489, 871, 1008, 1402, 3736
^{1}HOOClO-2	109.8, 446.0, 506.6	125, 271, 356, 452, 503, 874, 995, 1411, 3732
^{3}HOOClO-1	70.4, 881.4, 951.9	76, 79, 96, 207, 349, 845, 1188, 1462, 3523
^{3}HOOClO-2	40.9, 1083.3, 1124.2	43, 69, 78, 106, 200, 852, 1177, 1446, 3614
^{3}HOOClO-3	37.3, 1107.2, 1144.5	28, 78, 85, 122, 185, 846, 1179, 1446, 3604
^{1}HOClO$_2$	194.9, 214.8, 362.1	97, 373, 409, 534, 619, 1059, 1137, 1237, 3742
^{3}OOHOCl($^3A''$)	136.0, 1063.9, 1199.9	4, 18, 64, 87, 177, 743, 1281, 1647, 3763
^{1}OOHOCl($^1A'$)	78.5, 1160.3, 1238.8	22, 40, 75, 168, 294, 743, 1327, 1631, 3690
^{3}OHOClO-1($^3A''$)	136.1, 830.6, 966.7	23, 26, 108, 287, 352, 458, 967, 1114, 3681
^{3}OHOClO-2	218.2, 372.8, 534.5	86, 140, 202, 336, 490, 660, 944, 1270, 3622
TS1	101.6, 452.8, 499.4	300i, 169, 320, 392, 550, 813, 1010, 1359, 3763
TS2	145.5, 385.2, 462.4	417i, 174, 277, 364, 478, 798, 973, 1184, 3748
TS3	136.0, 395.6, 516.4	134i, 198, 348, 468, 542, 964, 1021, 1432, 3676
TS4	145.4, 369.5, 508.9	789i, 230, 250, 505, 526, 854, 1205, 1465, 2023
TS5	104.1, 356.8, 454.7	912i, 238, 300, 361, 462, 658, 877, 1009, 3796
TS6 ($^3A''$)	79.5, 662.2, 741.8	881i, 63, 175, 266, 352, 430, 1015, 1019, 3758
TS7	35.1, 671.8, 700.9	844i, 122, 133, 227, 351, 575, 851, 1006, 3767
TS8 ($^3A''$)	32.6, 716.7, 749.3	823i, 36, 90, 154, 326, 495, 939, 1033, 3762
TS9	169.4, 443.3, 524.9	689i, 115, 148, 388, 689, 818, 1027, 1127, 2011
TS10 ($^3A''$)	166.7, 350.8, 517.6	903i, 127, 233, 369, 543, 638, 682, 1411, 2830

TABLE 5: Heats of Formation of Four Species (kcal/mol) at 0 K Predicted at the G2M(CC2)//B3LYP/6-311+G(3df,2p) Level

species	this work[a]	literature
HOCl ($^1A'$)	−16.8	−17.1 ± 0.5,[b] −16.7 ± 0.6[c]
HOO ($^2A''$)	2.2	1.2 ± 2.0,[b] 4.0 ± 0.8,[d] 3.5 ± 0.5[e]
HOClO$_2$	0.1	4.2[f]
^{1}HOOClO-1	20.6	25.3[f]

[a] Heats of formation of OH, OClO, O_2($^1\Delta_g$), and ClO are 8.8 ± 0.1, 23.9 ± 1.9, 22.5, and 24.2 kcal/mol, respectively, as standard values taken from refs 23, 17, and 20, respectively. [b] Reference 17. [c] Reference 25. [d] Reference 26. [e] Reference 27. [f] Reference 24.

the forming O1−O5 bond length is 0.640 Å shorter than that in ^{3}OHOClO-2 and the breaking O1−Cl2 bond lengthens 0.183 Å compared with that in ^{3}OHOClO-2. As the reaction proceeds, O_2 eliminates from ^{3}OHOClO-2 to form ^{3}OOHOCl, which is a hydrogen-bonding complex formed by $^3O_2$ and HOCl. The complex lies below $^3O_2$ and HOCl by only 1.2 kcal/mol at the G2M level. The forward and reverse potential barriers for TS9 are 37.4 and 9.7 kcal/mol, respectively, and those for TS10 are 19.5 and 101.3 kcal/mol, respectively.

On the basis of the above discussion, we may conclude that the products HOO, ClO, HOCl, and $^1O_2$ are mainly produced by singlet reaction channels. Due to their high entrance barriers, the contribution of triplet channels to the overall reaction of the HO + OClO reaction can be neglected in kinetic modeling.

To establish the reliability of this calculation, the predicted heats of formation of some species are compared in Table 5 with the experimental and theoretical values reported previously by other authors. It can be seen that the values of HOCl and HOO calculated at the G2M level agree reasonably with experimental data and the absolute differences between the experimental and calculated values are less than 1.8 kcal/mol. However, for the heats of formation of HOClO$_2$ and HOOClO-

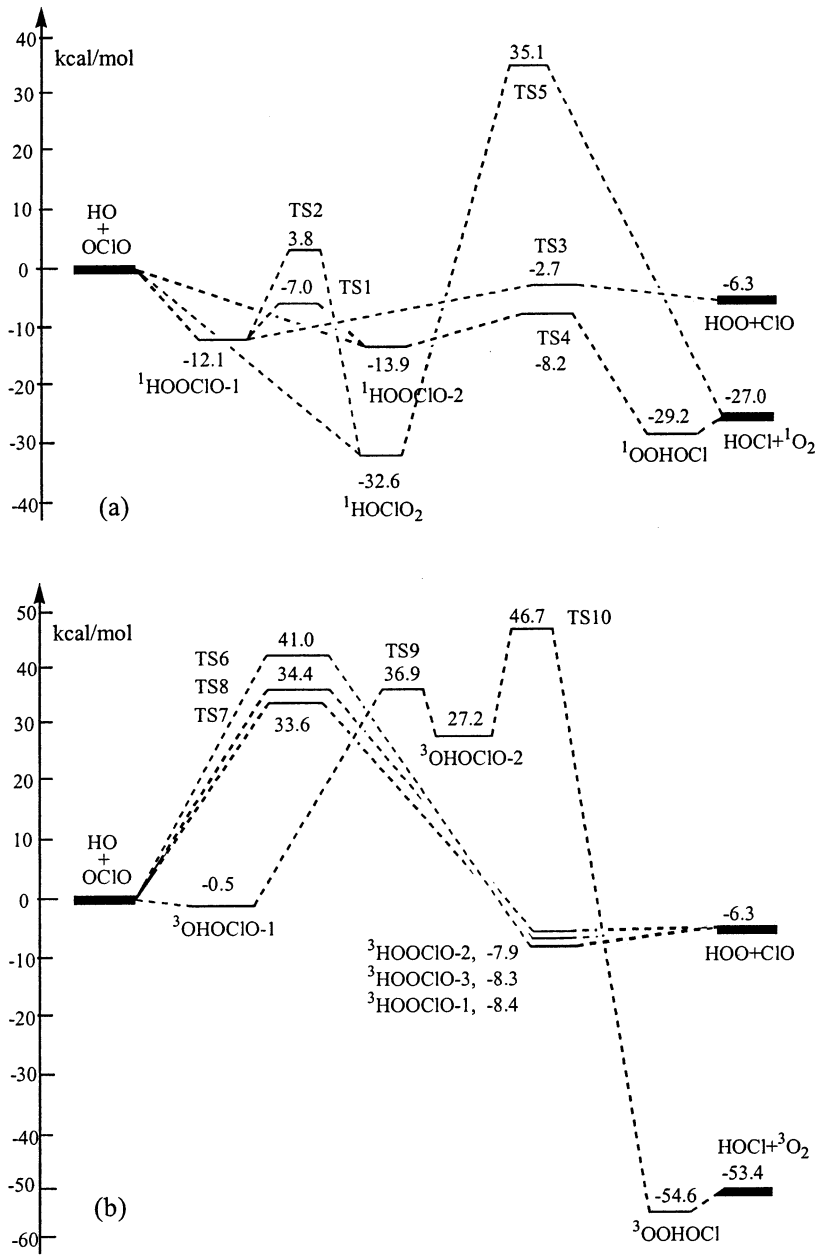

Figure 3. Schematic energy diagram of the OH + OClO system calculated by means of the G2M(CC2) method with the geometry parameters optimized at the B3LYP/6-311+G(3df,2p) level.

1, the G2M values are 4.1 and 4.7 kcal/mol less than those calculated by Francisco and Sander[24] at the G2 level, presumably due to the smaller basis set employed in geometry optimization with the latter method.

B. Rate Constant Calculations. From the above analysis of the reaction mechanism, key product channels of the HO + OClO reaction system can be determined as

$$\mathrm{HO + OClO \rightarrow {}^1HOOClO\text{-}1 \rightarrow HOO + ClO} \quad (1)$$

$$\uparrow\downarrow$$

$$\rightarrow {}^1\mathrm{HOOClO\text{-}2 \rightarrow HOCl + {}^1O_2} \quad (2)$$

$$\rightarrow {}^1\mathrm{HOClO_2} \quad (3)$$

The rate constants for these reaction channels were calculated by using variational TST and RRKM rate theory with parabolic barrier tunneling correction.[28] In fact, the tunneling effect is very small and unimportant because of the low-lying barriers below the reactants and the flat PES in the TS's involving H-atom migration. The increase in the rate constant due to tunneling is less than 2% at 200 K.

The relative energies given in Table 3 and the vibrational frequencies and moments of inertia in Table 4 are used to calculate the rate constants. The L−J (Lennard-Jones) parameters required for the RRKM calculations for the HOOClO isomers (assumed to be the same for all three), $\epsilon = 230$ K and $\sigma = 4.2$ Å, were derived from deconvoluting the L−J potential of the He−HOOClO system obtained by our ab initio calculation at the B3LYP/6-311G(d,p) level using the approximation, $\epsilon_{12} = (\epsilon_1\epsilon_2)^{1/2}$ and $\sigma_{12} = (\sigma_1+\sigma_2)/2$, for the collision pair. The ϵ_{12} and σ_{12} parameters for the He−HOOClO collision pair were predicted to be 48.0 K and 3.4 Å by fitting the He−HOOClO potential energy curve using the L−J function,[29] $V = 4\epsilon[(\sigma/r)^{12} - (\sigma/r)^6]$; here r represents the distance between atom He and the center of the mass of the intermediate. The L−J

SCHEME 1

$$\mathrm{OH + OClO} \leftrightarrow \mathrm{HOOClO\text{-}1^*} \rightarrow \mathrm{HOOClO\text{-}1\ (+M)}$$

$$\xrightarrow{k_1'} \mathrm{HO_2 + ClO}$$

$$\leftrightarrow \mathrm{HOOClO\text{-}2^*} \xrightarrow{k_2'} \mathrm{HOCl + {}^1O_2}$$

$$\rightarrow \mathrm{OH + OClO}$$

$$\rightarrow \mathrm{HOOClO\text{-}2\ (+M)}$$

SCHEME 2

$$\mathrm{OH + OClO} \leftrightarrow \mathrm{HOOClO\text{-}2^*} \rightarrow \mathrm{HOOClO\text{-}2\ (+M)}$$

$$\xrightarrow{k_2''} \mathrm{HOCl + {}^1O_2}$$

$$\leftrightarrow \mathrm{HOOClO\text{-}1^*} \rightarrow \mathrm{HOOClO\text{-}1\ (+M)}$$

$$\xrightarrow{k_1''} \mathrm{HO_2 + ClO}$$

$$\rightarrow \mathrm{OH + OClO}$$

parameters for He, $\epsilon = 10$ K and $\sigma = 2.56$ Å, were taken from the literature.[30]

The back-dissociation of ^{1}HOOClO-1, ^{1}HOOClO-2, and $HOClO_2$ intermediates to HO + OClO occurs barrierlessly, without a well-defined transition state. Their dissociation potential energy curves were calculated by varying the O3−O4, O3−O4, and Cl2−O4 bond distances with an interval of 0.1 Å for ^{1}HOOClO-1, ^{1}HOOClO-2, and $HOClO_2$ from their equilibrium values, 1.386, 1.314, and 1.783 Å, to 3.3, 3.2, and 3.5 Å, respectively. Other geometric parameters were fully optimized at the B3LYP/6-311G(d,p) level of theory. For each process, the B3LYP/6-311G(d,p) calculated total energy at each point along the reaction path was used to evaluate the Morse potential energy function and then scaled to match the dissociation energy predicted at the G2M level of theory. For the above processes, Morse's parameters β, obtained by fitting the predicted $V(r)$ curves, are 5.38, 4.07, and 3.71 Å^{-1}, respectively. The fitting deviations are less than 4% for the disassociation energy and 8% for β, which have no noticeable influence on the predicted rate constants.

The rate constant for the association reaction channel 3 was calculated in the temperature range from 200 to 2500 K and the pressure range from 1×10^{-5} to 7.6×10^{7} Torr with the VARIFLEX code,[14] whereas those for channels 1 and 2 were computed with the ChemRate code[16] coupling all intermediates involved in the forward and reverse reactions, as shown in Schemes 1 and 2. To perform the ChemRate calculation, we first evaluated the transition state structures for the barrierless association/decomposition processes by the much-practiced canonical variational method.[31−33] The Gibbs free energy of activation, $\Delta G(T,s)$, was calculated along the reaction path, s, using the energies given by the Morse functions and the optimized molecular structures and vibrational frequencies evaluated above. The transition state at the dividing surface $s = s^{\#}$ was defined by the maximum value of $\Delta G(T,s=s^{\#}) = \Delta G^{\#}(T)$ for each temperature.[32,33] For both barrierless association processes, the O(3)−O(4) separations of the variational transition states were determined to be 1.9 Å below 1500 K and 1.8 Å above 1500 K. Namely, the positions of the variational transition state for these two barrierless association processes are not sensitive to the variation of temperature.

The individual and total rate constant curves are presented in Figure 4 as a function of reciprocal temperature. From the result, it is evident that all rate constants exhibit negative temperature dependences at temperatures below 1000 K, and the rate constants for reaction channels 1 and 2 are pressure independent up to 1000 atm, whereas the rate constant for channel 3 is strongly positive-pressure dependent. Under the 1 Torr condition employed by Poulet et al.,[5] k_3 is far less than those of other channels and its contribution to total rate constant is negligible. Total rate constant calculated at 1 Torr pressure is shown in Figure 4d. The predicted rate constant is in good agreement with the available experimental data. The upswing in the total rate constant above 1000 K results from the increase in both k_1 and k_2 (see Figure 4a,b and Table 6). The predicted rate constants over the temperature range 200−1000 K at 1 Torr He pressure for the three product channels can be expressed in units of cm^3 molecule^{-1} s^{-1} by

$$k_1(T) = 1.22 \times 10^{-22} T^{2.75} \exp(1682/T)$$

$$k_2(T) = 5.47 \times 10^{-20} T^{2.07} \exp(2064/T)$$

$$k_3(T) = 1.37 \times 10^{4} T^{-6.61} \exp(-536/T) \qquad 200-500\ \mathrm{K}$$

$$k_3(T) = 4.99 \times 10^{54} T^{-22.36} \exp(-9807/T) \qquad 500-1000\ \mathrm{K}$$

$$k_{\mathrm{tot}}(T) = 1.78 \times 10^{-20} T^{2.25} \exp(2100/T)$$

For AP combustion applications, the high- and low-pressure limits of the rate constant for the formation of $HClO_3$ from OH + OClO, k_3, with N_2 as the third-body are given as

$$k_3^{\infty}(T) = 3.24 \times 10^{-11} T^{0.28} \exp(-18/T)$$

cm^3 molecule^{-1} s^{-1} in 200−2500 K

and

$$k_3^{0}(T) = 1.28 \times 10^{-13} T^{-6.36} \exp(-635/T)$$

cm^6 molecule^{-2} s^{-1} in 200−800 K

$$k_3^{0}(T) = 7.37 \times 10^{84} T^{-36.02} \exp(-22134/T)$$

cm^6 molecule^{-2} s^{-1} in 800−1000 K

$$k_3^{0}(T) = 2.91 \times 10^{-13} T^{-8.42} \exp(11500/T)$$

cm^6 molecule^{-2} s^{-1} in 1000−2500 K

At atmospheric N_2 pressure, k_3 can be represented by the expressions

$$k_3^{1\ \mathrm{atm}}(T) = 1.33 \times 10^{9} T^{-7.36} \exp(-1182/T)$$

cm^3 molecule^{-1} s^{-1} in 200−800 K

$$k_3^{1\ \mathrm{atm}}(T) = 5.03 \times 10^{115} T^{-39.55} \exp(-25443/T)$$

cm^3 molecule^{-1} s^{-1} in 800−1000 K

$$k_3^{1\ \mathrm{atm}}(T) = 3.89 \times 10^{10} T^{-9.76} \exp(10860/T)$$

cm^3 molecule^{-1} s^{-1} in 1000−2500 K

In contrast to the results above, the rate constants of the triplet reaction channel via the lowest barrier at TS7 shown in Figure 5 are many orders of magnitude smaller. Accordingly, the reactions via all triplet paths cannot compete with those via the singlet paths, as one would expect. As the absolute error of energies predicted by the G2M method for the second row compounds was estimated to be in the range 0.9−1.2 kcal/mol,[12] we have examined the sensitivity of the predicted total rate

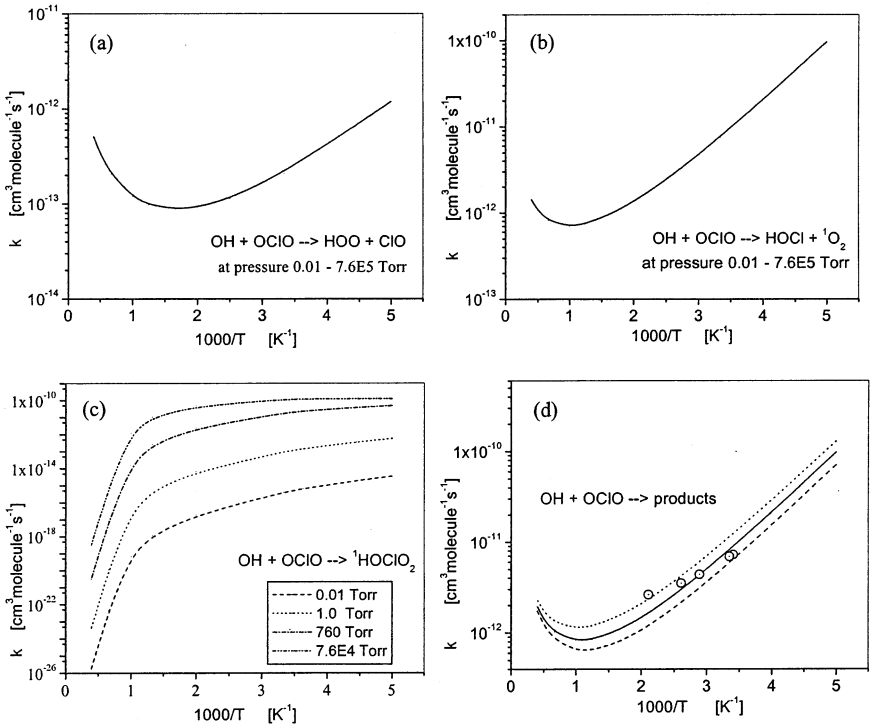

Figure 4. Plots of predicted individual and total rate constants. (a) Rate constants for production of HO_2 + ClO. (b) Rate constants for production of HOCl + $^1O_2$. (c) Rate constants for production of $HOClO_2$. (d) Comparison of predicted total rate constants with available experimental data: (solid curve) predicted k_{tot} at 1 Torr He; (dotted and dashed curves) predicted k_{tot} at 1 Torr He with the TS4 energy arbitrarily decreased or increased by 1.2 kcal/mol; (circles) experimental data.[5]

TABLE 6: Predicted Product Branching Ratios for Channels 1 and 2 at 1 Torr He Pressure (Rate Constants in Units of cm^3 molecule^{-1}s^{-1})

	HO_2 + ClO			HOCl + $^1O_2$			
T/K	k_1'	k_1''	$k_1 = k_1' + k_1''$	k_2'	k_2''	$k_2 = k_2' + k_2''$	$k_2/(k_1 + k_2)$
200	2.91E−13	9.01E−13	1.19E−12	9.60E−12	8.64E−11	9.60E−11	0.988
300	6.90E−14	1.40E−13	2.09E−13	1.34E−12	6.14E−12	7.48E−12	0.973
400	4.38E−14	6.96E−14	1.13E−13	5.59E−13	1.86E−12	2.42E−12	0.955
500	3.97E−14	5.21E−14	9.18E−14	3.56E−13	9.93E−13	1.35E−12	0.936
600	4.12E−14	4.67E−14	8.79E−14	2.78E−13	7.06E−13	9.84E−13	0.918
800	5.18E−14	4.58E−14	9.76E−14	2.23E−13	5.19E−13	7.42E−13	0.884
1000	6.89E−14	5.01E−14	1.19E−13	2.11E−13	4.87E−13	6.98E−13	0.854
1500	1.36E−13	6.99E−14	2.06E−13	2.35E−13	5.81E−13	8.16E−13	0.799
2000	2.40E−13	9.70E−14	3.37E−13	2.88E−13	7.80E−13	1.07E−12	0.760
2500	3.78E−13	1.30E−13	5.08E−13	3.69E−13	1.06E−12	1.43E−12	0.738

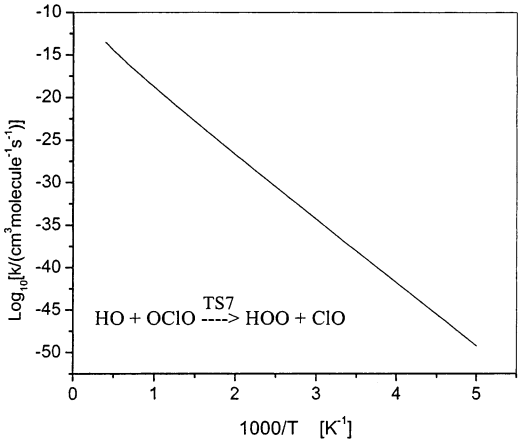

Figure 5. Plot of the rate constants of the triplet reaction channel HO + OClO → TS7 → HOO + ClO.

constant to the potential error in TS1 and TS4. The result of our test shows that k_{tot} is insensitive to the increase or decrease in the barrier at TS1 by 1.2 kcal/mol, becasuse the key intermediate leading to the formation of the major products HOCl + O_2, ^{1}HOOClO-2, can be formed by the direct barrierless association process. The increase or decrease in the TS4 barrier by the same amount, however, leads to a corresponding decrease in k_{tot} by 10−28% or increase by 17−42%, respectively, depending on the temperature, as shown in Figure 4d.

C. HOCl Branching Ratio. Experimentally, the branching ratio for the formation of HOCl at ∼1 Torr pressure was reported to be near unity, with the lower limit of 0.8, allowing for potential contributions from side reactions;[5] this is truly an interesting observation. The results of our calculation with ChemRate, based on the two possible entrance channels forming HOOClO-1* and HOOClO-2* as shown above, allowing for all forward and reverse reactions, are summarized in Table 6 and graphically presented in Figure 6a−d including the contribution from reaction 3 forming $HOClO_2$, which is competitive only at higher pressures. As revealed by the results, the branching ratio for the formation of HOCl + O_2 under the conditions employed by Poulet et al.[5] (293−473 K, 0.5−1.4 Torr) was indeed near unity; at 300 K, about 80% derives from the reaction via HOOClO-2* and about 17% from HOOClO-

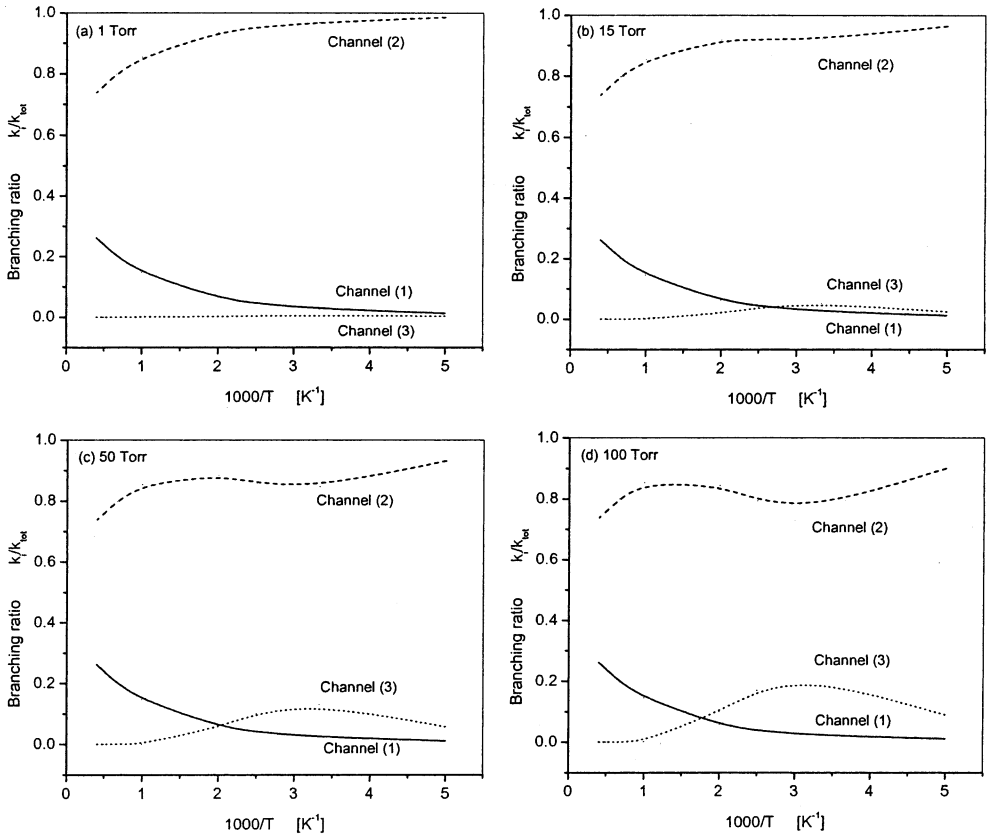

Figure 6. Product branching ratios predicted for different *T*, *P* conditions.

1* via the isomerization process. At higher pressures, under which no experimental data are available, the branching ratio for HOCl formation was affected by pressure and temperature, due to the formation of $HOClO_2$, which is strongly *P*, *T*-dependent (see Figure 6c,d). It should be mentioned that in our ChemRate calculations, the reaction time used in the solution of the master equation covered the range 0.001−10 ms. The predicted absolute rate constants for the individual channels are independent of time.

4. Conclusions

The mechanism for the OH + OClO reaction over the singlet and triplet potential energy surfaces of the OH + OClO reaction have been elucidated at the G2M(CC2)//B3LYP/6-311+G(3df,-2p) level of theory. Three major product channels, (1) HOO + ClO, (2) HOCl + $^1O_2$, and (3) $^1HOClO_2$, have been identified on the singlet PES. The rate constants for formation of these products have been calculated in the temperature range from 200 to 2500 K and the pressure range from 1×10^{-5} Torr to 7.6×10^7 Torr by using variational RRKM theory with the VARIFLEX and ChemRate programs. The predicted results show that the rate constants of channels 1 and 2 are pressure independent up to 1000 atm and that of channel 3 has a strong pressure dependence. The theoretically predicted near unity branching ratio for formation of the HOCl + $^1O_2$ products and the total rate constant at 1 Torr He pressure in the 300−500 K range agrees well with experimental data. Because of the high entrance barriers of all triplet channels, their contributions to the OH + OClO reaction are negligible kinetically.

Acknowledgment. This work is sponsored by the Office of Naval Research under contract no. N00014-02-1-0133, Dr. J. Goldwasser program manager. M.C.L. acknowledges Taiwan's National Science Council for the distinguished visiting professorship at the National Chiaotung University in Hsinchu.

References and Notes

(1) Grothe, H.; Willner, H. *Angew. Chem.* **1994**, *106*, 1581.
(2) Zhu, R. S.; Lin, M. C. *PhysChemComm* **2001**, *25*, 1.
(3) Birks, J. W.; Shoemaker, B.; Leck, T. J.; Borders, R. A.; Hart, L. J. *J. Chem. Phys.* **1977**, *66*, 4591.
(4) Wongdontri-Stuper, W.; Jayanty, R. K. M.; Simonaitis, R.; Heicklen, J. *J. Photochem.* **1979**, *10*, 163.
(5) Poulet, G.; Zagogianni, H.; Le Bras, G. *Int. J. Chem. Kinet.* **1986**, *18*, 847.
(6) Zhu, R. S.; Xu, Z. F.; Lin, M. C. *J. Chem. Phys.* **2002**, *116*, 7452.
(7) Zhu, R. S.; Lin, M. C. *J. Phys. Chem. A* **2002,** *106*, 8386.
(8) Zhu, R. S.; Lin, M. C. *J. Chem. Phys.*, in press.
(9) (a) Becke, A. D. *J. Chem. Phys.* **1993**, *98*, 5648. (b) Becke, A. D. *J. Chem. Phys.* **1992**, *96*, 2155. (c) Becke, A. D. *J. Chem. Phys.* **1992**, *97*, 9173.
(10) Lee, C.; Yang, W.; Parr, R. G. *Phys. Rev.* **1988**, *37B*, 785.
(11) (a) Gonzalez, C.; Schlegel, H. B. *J. Chem. Phys.* **1989**, *90*, 2154. (b) Gonzalez, C.; Schlegel, H. B. *J. Phys. Chem.* **1990**, *94*, 5523.
(12) Mebel, A. M.; Morokuma, K.; Lin, M. C. *J. Chem. Phys.* **1995**, *103*, 7414.
(13) Frisch, M. J.; Trucks, G. W.; Schlegel, H. B.; Scuseria, G. E.; Robb, M. A.; Cheeseman, J. R.; Zakrzewski, V. G.; Montgomery, J. A., Jr.; Stratmann, R. E.; Burant, J. C.; Dapprich, S.; Millam, J. M.; Daniels, A. D.; Kudin, K. N.; Strain, M. C.; Farkas, O.; Tomasi, J.; Barone, V.; Cossi, M.; Cammi, R.; Mennucci, B.; Pomelli, C.; Adamo, C.; Clifford, S.; Ochterski, J.; Petersson, G. A.; Ayala, P. Y.; Cui, J.; Morokuma, K.; Malick, D. K.; Rabuck, A. D.; Raghavachari, K.; Foresman, J. B.; Cioslowski, J.; Ortiz, J. V.; Baboul, A. G.; Stefanov, B. B.; Liu, G.; Liashenko, A.; Piskorz, P.; Komaromi, I.; Gomperts, R.; Martin, R. L.; Fox, D. J.; Keith, T.; Al-Laham, M. A.; Peng, C. Y.; Nanayakkara, A.; Gonzalez, C.; Challacombe, M.; Gill, P. M. W.; Johnson, B.; Chen, W.; Wong, M. W.; Andres, J. L.; Gonzalez, C.; Head-Gordon, M.; Replogle, E. S.; Pople, J. A. *Gaussian 98*; Gaussian, Inc.: Pittsburgh, PA, 1998.
(14) Klippenstein, S. J.; Wagner, A. F.; Dunbar, R. C.; Wardlaw, D. M. and Robertson, S. H. *VARIFLEX: VERSION 1.00*, 1999.
(15) Wardlaw, D. M.; Marcus, R. A. *Chem. Phys. Lett.* **1984**, *110*, 230; *J. Chem. Phys.* **1985**, *83*, 3462. Klippenstein, S. J. *J. Chem. Phys.* **1992**, *96*, 367. Klippenstein, S. J.; Marcus, R. A. *J. Chem. Phys.* **1987**, *87*, 3410.

(16) Mokrushin, V.; Bedanov, V.; Tsang, W.; Zachariah, M. R.; Knyazev, V. D. *ChemRate, Version 1.19*; National Institute of Standards and Technology: Gaithersburg, MD 20899, 2002.

(17) Chase, M. W., Jr. NIST-JANAF Thermochemical Tables, 4th ed. *J. Phys. Chem. Ref. Data* **1998**, Monograph No. 9.

(18) Uehara, H.; Kawaguchi, K.; Hirota, E. *J. Chem. Phys*. **1985**, *83*, 5479.

(19) Escribano, R. M.; Lonnardo, G. D.; Fusina, L. *Chem. Phys. Lett.* **1996**, *259*, 614.

(20) Huber, K. P.; Herzberg, G. *Molecular Spectra and Molecular Structure*. *IV. Constants of Diatomic Molecules*; Van Nostrand Reinhold Co.: New York, 1979.

(21) Azzolini, C.; Cavazza, F.; Crovetti, G.; Dilonardo, G.; Frulla, R.; Escribano, R.; Fusina, L. *J. Mol. Spectrosc.* **1994**, *168*, 494.

(22) (a) Yamada, C.; Endo, Y.; Hirota, E., *J. Chem. Phys*. **1983**, *78*, 4379. (b) Burkholder, J. B.; Hammer, P. D.; Howard, C. J.; Towle, J. P.; Brown, J. M., *J. Mol. Spectrosc.* **1992**, *151*, 493.

(23) Ruscic, B.; Feller, D.; Dixon, D. A.; Peterson, K. A.; Harding, L. B.; Asher, R. L.; Wagner, A. F. *J. Phys. Chem. A* **2001**, *105*, 1.

(24) Francisco, J. S.; Sander, S. F. *J. Phys. Chem.* **1996**, *100*, 573.

(25) Barnes, R. J.; Sinha, A. *J. Chem. Phys.* **1997**, *107*, 3730

(26) Litorja, M.; Ruscic, B. *J. Electron Spectrosc. Relat. Phenom.* **1998**, *97*, 131.

(27) Bauschlicher, C. W., Jr.; Partridge, H. *Chem. Phys. Lett*. **1993**, *208*, 241.

(28) Bell, R. P. *The Tunnel Effect in Chemistry*; Chapman and Hall Ltd.: London, 1980.

(29) Hirschfelder, J. O.; Curtiss, C. F.; Bird, R. B. *Molecular theory of gases and liquids*, 2nd ed.; John Wiley and Sons Inc.: New York, 1964.

(30) Woo, C.-W. in *The Physics of Liquid and Solid Helium*; Bennemann, K. H., Ketterson, J. B., Eds.; Wiley: New York, 1981.

(31) Isaacson, A. D.; Truhlar, D. C. *J. Chem. Phys*. **1982**, *76*, 1380.

(32) Hsu, C.-C.; Mebel, A. M.; Lin, M. C. *J. Chem. Phys*. **1996**, *105*, 2346.

(33) Chakraborty, D.; Hsu, C.-C.; Lin, M. C. *J. Chem. Phys*. **1998**, *109*, 8889.